Numerical Modeling of Oil-Jet Lubrication for Spur Gears using Smoothed Particle Hydrodynamics

Marc C. Keller, Samuel Braun, Lars Wieth, Geoffroy Chaussonnet, Thilo Dauch,
Rainer Koch, Corina Höfler, Hans-Jörg Bauer

Institut für Thermische Strömungsmaschinen

Karlsruhe Institute of Technology (KIT)

Karlsruhe, Germany

marc.keller@kit.edu

Abstract—**Understanding and optimizing the lubrication and cooling in aero engine gearbox applications is crucial for a reliable and efficient sub-system design of future aircraft engines. Due to the complex design of gearboxes with its various rotating parts, space and access for experimental investigations are severely limited. Thus, suitable numerical methods need to be developed in order to thoroughly investigate the evolving oil-air two-phase flow in the vicinity of the gear teeth.**

In this paper, the impingement of a single oil-jet on a single rotating spur gear was analyzed using the Smoothed Particle Hydrodynamics (SPH) method. The study was conducted with a simplified 2D setup under typical operating conditions met in reduction gear units of novel large civil aircraft engines.

Results of the predicted oil-air two-phase flow are presented and compared to conventional Volume-of-Fluid (VOF) simulations. The wetting behavior and the impingement depth of the oil-jet between the gear teeth are investigated for varying oil-jet velocities and rotational speeds. In order to capture three-dimensional flow effects, a 3D setup and preliminary results are presented.

Fig. 1. Generic spur gear (left) and area of interest in the vicinity of the oil-jet injection (right).

I. INTRODUCTION

Air traffic undergoes a rapid growth within the next decades and at the same time environmental pollution is a major problem. Thus, to achieve the ambitious goals of future emission restrictions for aircrafts, new jet engine concepts need to be developed. By placing a reduction gearbox in between the fan and the low pressure spool of the core engine, the bypass ratio of large civil aircraft engines can be further increased while optimized operating conditions for both components can be realized. In this way, the overall engine efficiency will be improved, leading to reduced fuel consumption and hence to fewer emissions. Furthermore, noise and weight will be reduced, making the geared turbofan even more promising for next generation aero-engines.

The key component of this technology is the planetary reduction gearbox, which requires a high transmission efficiency to meet the overall targets. Thus, a sophisticated cooling and lubrication system is essential, as high mechanical and thermal loads occur. For high-speed gears oil-jet lubrication is usually applied, where small oil-jets are targeted onto the gear or into the gear meshing (see Fig. 1). The evolving two-phase flow plays a key role for the cooling and lubrication process.
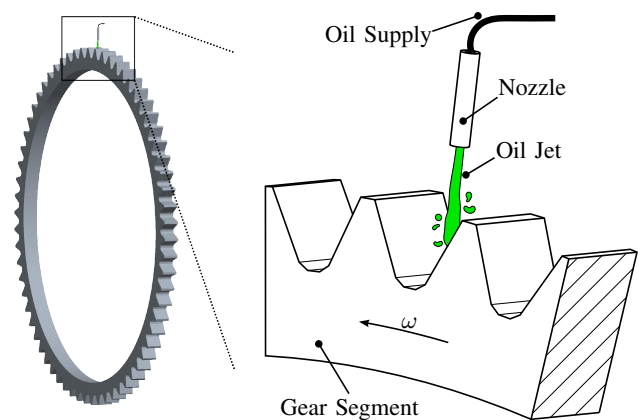
Therefore, it is crucial to correctly predict the multiphase flow in such a gearbox.

In the past, oil-jet lubrication has mainly been investigated experimentally as presented by Akin et al. [1] or Handschuh [2]. However, due to poor accessibility, high fluid velocities and complex flow patterns of the prevailing two-phase flow, experimental methods are limited. This is why numerical methods are essential to gain detailed insights into the complex oil-gear interaction.

Only few publications address the issue by means of numerical methods. In [3] and [4] the two-phase flow is predicted using the Eulerian Volume-of-Fluid (VOF) method in combination with an adaptive mesh refinement (AMR) technique to thoroughly capture the phase interface. The gear rotation is included by additional mesh manipulation steps, which are inevitably required for mesh-based methods and which are frequently mentioned to be origin of numerical problems and computational overhead, particularly for parallel processing. Thus, the SPH method is a promising alternative, as it enables a much easier modeling of complex deforming domains and the phase interface is transported inherently.

The aim of the present work is to use the Smoothed Particle Hydrodynamics (SPH) method to predict the detailed

69

oil-gear interaction in the vicinity of the oil-jet injection. While Mettichi et al. [5] applied SPH to general single-phase oil flows in complete gearbox systems, the present paper aims to investigate two-phase flow phenomena on a smaller length scale. As a first step, the impingement of a single oil-jet on a single rotating spur gear is analyzed as depicted in Fig. 1. Therefore, a generic two-dimensional setup was defined and analyzed regarding the impingement depth and wetting behavior. A comparison to conducted VOF simulations underlines the validity of the results.

II. METHODOLOGY

The investigated flow configuration is demanding for computational methods, due to the fact that besides a complex two-phase flow it also involves a deforming computational domain due to relative movement between the gear and the nozzle. The SPH and the state-of-the-art VOF method offer fundamentally different boundary conditions (BCs) for the numerical modeling of such flow problems. The basic formulations of both methods and implementation details of the gear motion are explained subsequently.

A. SPH Model

At the "Institut für Thermische Strömungsmaschinen" (ITS) a highly parallelized weakly-compressible SPH code has been developed [6]. The code was recently applied to technical systems like aero engine bearing chambers [7], homogenizers [8], or liquid fuel atomizers ([9], [10]), demonstrating its applicability for industrially relevant cases. The following purely Lagrangian SPH formulation of the discretized Navier-Stokes equations, assuming an isothermal flow, is used:

$$\begin{cases} \langle \rho \rangle_a = m_a \sum_b W_{ab,h} \\ \left\langle \dfrac{D\vec{u}}{Dt} \right\rangle_a = \left\langle \vec{f} \right\rangle_{a,p} + \left\langle \vec{f} \right\rangle_{a,\nu} + \left\langle \vec{f} \right\rangle_{a,\text{SF}} + \left\langle \vec{f} \right\rangle_{a,\text{b}} \\ p_a = \dfrac{\rho_{0,a} c_a^2}{\gamma_a} \left[\left(\dfrac{\rho_a}{\rho_{0,a}} \right)^{\gamma} - 1 \right] + p_{\text{back}} \end{cases} \quad (1)$$

The density ρ of particle a is evaluated directly from the position of its neighboring particles b within the sphere of influence $r_{\max}$ as proposed by Hu and Adams [11] for multi-phase flows with high density ratios. In the same relation m is the mass of the particle and $W_{ab,h}$ the kernel function. Here, a quintic spline is used with the smoothing length $h = \Delta x$ and $r_{\max} = 3h$, where Δx represents the mean particle spacing.

The second line in (1) represents the momentum equation, where $\vec{u}$ is the particle velocity vector. The RHS contains the forces acting on the particle. In the order of appearance, the different contributors are due to pressure, viscosity, surface tension, and all remaining external body forces.

For the pressure gradient the locally conservative form as stated by Colagrossi and Landrini [12] is applied. Viscous stress is modeled according to Szewc et al. [13]. Surface tension is a particular contributor in the momentum equation

of multi-phase flows. The used model is of the continuum surface force type and derived from Adami et al. [14].

Closure of the system of equations is achieved by calculating the pressure directly from the density via the equation of state specified last in (1). $\rho_{0,a}$ is the reference density, c_a the artificial speed of sound, γ the polytropic exponent, and p_{back} the background pressure. By setting the speed of sound to approximately 10 times $|\vec{u}_{\max}|$ the weakly compressible assumption ($\Delta \rho / \rho \leq 1\,\%$) is ensured.

Inlet, outlet, wall, and periodic BCs are required to model real flow problems. Here, the framework as previously reported by Braun et al. [15] is adapted. Walls are modeled by three layers of wall particles and inlet, outlet, and periodic BCs are incorporated by so-called markers. For details it is referred to [15].

The gear motion was incorporated by a universal body motion feature. A translational and rotational motion can be prescribed to each body, a defined set of wall particles. The position and velocity of each particle in a body is then calculated directly from the superposition of the prescribed translational and rotational motion. Thereby, the center of a body is tracked separately, which is used to calculated the rotation matrix once for each time step and body. Hence, the computational overhead of this feature is low ($< 1\,\%$). Furthermore, it allows incorporating the gear rotation in combination with periodicity.

Limitations of this implementation arise when parallel execution is performed. Due to the deformation of the fluid domain a static load balance algorithm executed at the beginning of the simulation might not give the best partitioning at later time steps, leading to an unequal distribution of particles between the subdomains and to increased computational time. This could be avoided by a dynamic load balancing (see [16]).

B. VOF Model

In this work, the commercial software ANSYS® Fluent, Release 16.1 was used for simulations with the mesh-bashed VOF method. The two-phase flow is modeled using the *implicit* formulation of the volume fraction; for spatial discretization the *Compressive* scheme is used. Gradients are spatially discretized by means of the *Least Square Cell Based* and pressure by the *PRESTO!* scheme. Further, the *PISO* scheme is applied for the pressure-velocity coupling. The transient discretization is set to *Second Order Implicit*. The reader is referred to [17] for details of the models.

For the transient simulation with deforming computational domain the initial mesh must be adapted after each time step to account for the gear motion. The strategies which have been applied to overcome this problem in the past are the sliding interface [3], smoothing, re-meshing [4], or over-set [18] method. In addition, combinations of these techniques were applied [19]. Extensive computational effort must be accepted with either of the methods, since interpolation and mesh manipulation are involved. Furthermore, interpolating between modified meshes is prone to numerical errors and mesh smoothing or re-meshing can lead to deficient mesh quality.
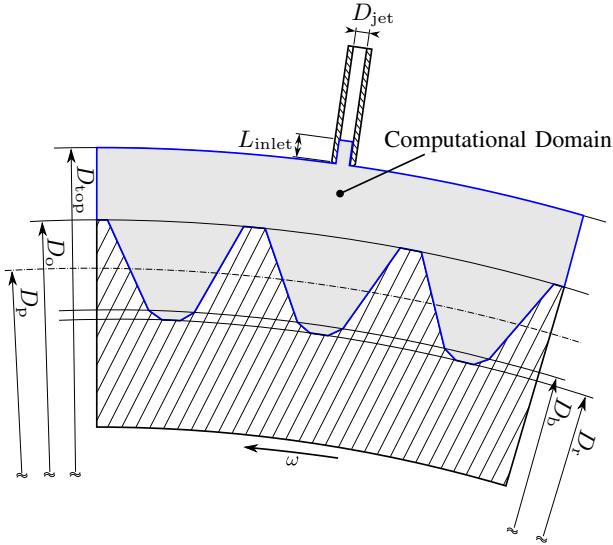
Fig. 2. Cross section through center plane of the extracted segment containing three teeth and computational domain of the two-dimensional setup (blue).

Property	Symbol	Value [D_{jet}]
Jet diameter	D_{jet}	1
Segment outer diameter	D_{top}	254.8
Pitch diameter	D_p	237.4
Outer diameter	D_o	244.1
Base diameter	D_b	230.9
Root diameter	D_r	229.7
Inlet duct length	L_{inlet}	2
Gear width	L_{width}	10

For the problem at hand, the sliding interface approach is most promising. Its idea is to split the mesh into two parts, in this case a static and a rotating annulus, which then move relative to each other along a well defined interface. Hence, the two mesh zones do not need to be modified, but only the values at the interface are interpolated and exchanged. Note that this method would not be applicable for a setup with two interlocking gears, since there would be no well defined interface.

III. NUMERICAL SETUP

The investigated setup consists of a radially injected oil-jet which hits the teeth of a rotating spur gear centric (see Fig. 1). While the nozzle is fixed in space, the gear rotates with the angular speed ω, resulting in an intermittent impingement of the oil-jet on the gear flanks.

A. Geometry

To reduce the computational effort, a circumferential segment of the full gear was extracted. Since only a few impacts of the jet on the gear flanks are sufficient for the current investigations, a segment consisting of 3 teeth was chosen. This facilitates high-resolution simulations in the area of interest, omitting the parts of the full domain where no oil is present. The extracted segment coincides with the right view in Fig. 1; the cross section through the center plane is depicted in Fig. 2.

For the present work a generic spur gear was defined. Its physical dimensions and further geometrical properties introduced in Fig. 2 are listed in Tab. I. The gear exhibits all relevant geometrical features of common spur gears. The simplified piecewise linear modeling of the teeth fillet and the gear flank is assumed to not significantly change the general flow behavior.

To further decrease computational effort a two-dimensional setup is investigated at first.

B. Boundary Conditions

The confining boundaries of the fluid domain are represented by blue lines in Fig. 2. The interior of the nozzle is not fully modeled, but only a length of twice the jet diameter. Another simplification is the upper confinement of the domain in radial direction. There is no distinct physical border adjacent to the nozzle towards the ambient environment. However, the upper confinement was modeled with a circular outlet at $d = D_{top}$. This procedure enables an easy modeling without affecting the physics in the area of interest near the gear surface.

For both, the SPH and the VOF method, the applied set of BCs is presented subsequently.

1) SPH: The computational domain and the BCs for the SPH simulations are shown in Fig. 3. The oil inlet was modeled by applying a uniform velocity profile with the magnitude V_{jet} in normal direction. For the static walls of the nozzle a no-slip BC was imposed. Pressure outlet BCs on each side of the nozzle confine the fluid domain in radial direction. On the left and right side of the domain rotational periodic BCs were set. The corresponding markers are placed along the orange curves. It should be noted that the area reaches beyond the fluid domain for the depicted situation. However, at a later time in the simulation the gear surface (ROTATING WALL) will cut the periodic (orange) lines at a different position. The marker placement as shown ensures that the intersection is always on the orange lines and thus facilitates correct periodic behavior. The aforementioned gear motion was incorporated by a rotating no-slip wall BC (see Sec. II-A) for the set of particles representing the gear surface. At the start of the simulation the interior is filled with air particles at rest.

2) VOF: As described in Sec. II-B the mesh-based VOF method requires a different incorporation of the gear motion. In the present work a sliding interface approach was applied in combination with periodic BCs. Figure 4 illustrates this setup, consisting of an outer static cell zone (light gray) and an inner rotating cell zone (dark gray), representing the gear and parts of the surrounding fluid domain. At initial
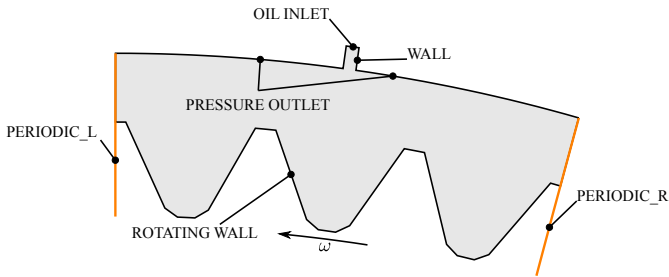
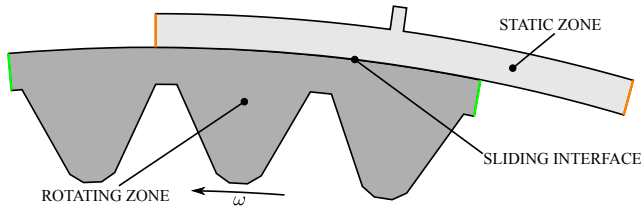Fig. 3.   Computational domain of the two-dimensional SPH setup.

Fig. 4.   Computational domain of the two-dimensional mesh-based VOF setup. The gear motion is incorporated by a sliding interface coupling the rotating (dark gray) and the static cell zone (light gray).

TABLE II
MATERIAL PROPERTIES OF THE MODELED FLUIDS.

Fluid	Density ρ [kg/m^3]	Dynamic Viscosity μ [kg/(m s)]
Air	0.9862	$21.010 \cdot 10^{-6}$
Mobil Jet Oil II	949	$7.896 \cdot 10^{-3}$

TABLE III
DIMENSIONLESS OPERATING CONDITIONS.

Parameter	Cases								
	I-a	I-b	I-c	II-a	II-b	II-c	III-a	III-b	III-c
n_{gear} [n_0]	$\frac{7}{8}$	$\frac{7}{8}$	$\frac{7}{8}$	1	1	1	$\frac{9}{8}$	$\frac{9}{8}$	$\frac{9}{8}$
V_{jet} [V_0]	$\frac{2}{3}$	1	$\frac{4}{3}$	$\frac{2}{3}$	1	$\frac{4}{3}$	$\frac{2}{3}$	1	$\frac{4}{3}$

time the two zones were placed such that the interfaces overlap completely. The sliding interface was implemented using the *Periodic Repeat* interface condition available in ANSYS® Fluent. This approach facilitates that a) values at the overlapping part of the two cell zones are interpolated and exchanged and b) the non-overlapping parts are coupled via a periodic-like BC, which retains the periodic character of the setup. Due to the divided domain the mesh-based setup also requires two circumferentially periodic BCs. One for the static (orange) and one for the rotating (green) cell zone, respectively. The remaining boundary and initial conditions were assigned equivalent to the SPH setup (see Fig.3).

Comparing the two setups clearly shows the advantages of SPH regarding the modeling of deforming computational domains. Whereas with the SPH method the gear motion can be defined directly for the relevant gear wall particles, the VOF method requires more complex modeling strategies.

C. Operating Conditions

A total of nine 2D cases have been investigated. The operating conditions were chosen similar to engine relevant conditions. For all cases the fluid properties were kept constant according to Tab. II. Mobil Jet Oil II is a typical engine oil used in aircraft industry. The oil and air properties were evaluated at an assumed temperature of $80\,^\circ\text{C}$ typically found in gearboxes. Although the fluids will undergo temperature changes due to heat pickup from the gear, density and viscosity changes were neglected in this study. The surface tension is $0.025\,\text{N/m}$ and a contact angle of 45° was imposed.

The specifications of the investigated system can be split into geometrically and operationally restricted operating parameters. Former are the oil-jet diameter, position of the nozzle, jet angle, or gear geometry. These properties were not

changed in this study. The operational parameters are the oil-jet velocity, rotational speed of the gear, and fluid properties. The first two parameters were varied in this work. As a baseline case the reference jet velocity V_0 and the reference rotational speed n_0 were defined, where the ratio of the jet velocity over the circumferential velocity at the pitch line $V_0/V_p \approx 0.5$ with $V_p = \pi D_p n_0$ was chosen. Based on the baseline conditions, V_{jet} and n_{gear} were varied in the range of $\pm 33\,\% \, V_0$ and $\pm 12.5\,\% \, n_0$, respectively as listed in Tab. III.

IV. RESULTS

First, the non-dimensional numbers defining the prevailing flow type are presented, as it allows a better interpretation of the SPH and VOF simulations. As detailed experimental data does not exist, a validation of the SPH method with experiments is not part of this paper. However, the SPH results are compared to the established VOF method to show accordance. Hence, the 2D results for the two-phase flow obtained by both methods are compared phenomenologically and with regard to computational costs. Thereafter, the predicted impingement depth is analyzed and compared to a kinematic model. As the wetting behavior on the gear flanks is of great interest for design purposes, it is also analyzed. Finally, the setup and the result of a three-dimensional SPH simulation are presented.

A. Dimensionless Groups

The investigated two-phase flow can be characterized by a set of dimensionless groups, which were evaluated for three operating points and can be found in Tab. IV.

1) Jet Disintegration: The injection of the oil into the surrounding air is similar to the processes taking place in pressure atomizers, for which it is known, that the Reynolds and Weber number defined by

$$\text{Re}_{\text{jet}} = \frac{V_{\text{jet}} D_{\text{jet}}}{\nu_{\text{oil}}} \quad \text{and} \quad \text{We}_{\text{jet}} = \frac{\rho_{\text{oil}} V_{\text{jet}}^2 D_{\text{jet}}}{\sigma} \quad (2)$$

mainly characterize the general flow and the disintegration mechanism [20]. Due to the interaction of the oil-jet with the

TABLE IV
DIMENSIONLESS GROUPS OF THE INVESTIGATED MULTI-PHASE PROBLEM.

Operating Point	$\mathrm{Re}_{\mathrm{jet}}$	$\mathrm{We}_{\mathrm{jet}}$	$\mathrm{Oh}_{\mathrm{jet}}$	$\mathrm{We}_{\mathrm{cf}}$	q
I-a	$2.76 \cdot 10^3$	$1.75 \cdot 10^4$	$4.78 \cdot 10^{-2}$	92	190
II-b (baseline)	$4.15 \cdot 10^3$	$3.93 \cdot 10^4$	$4.78 \cdot 10^{-2}$	120	327
III-c	$5.53 \cdot 10^3$	$6.98 \cdot 10^4$	$4.78 \cdot 10^{-2}$	152	459

surrounding air, the liquid phase is exposed to shear forces enforcing disintegration of the oil-jet. The jet breakup regime can be estimated by the Ohnesorge number

$$\mathrm{Oh}_{\mathrm{jet}} = \frac{\sqrt{\mathrm{We}_{\mathrm{jet}}}}{\mathrm{Re}_{\mathrm{jet}}} . \qquad (3)$$

For the operating points given in Tab. IV, the expected breakup regime was determined according to correlations proposed by Ohnesorge [21]. It was found, that no significant jet breakup is to be expected for the prevailing operating conditions.

2) Jet in Cross Flow: The estimation of the disintegration regime is only valid for ambient air at rest and does not include any temporal information. Since the air is accelerated by the rotating gear, the oil-jet is released into air which has a predominant velocity component in circumferential direction. Hence, the phenomena known from a jet in cross-flow can be transferred to the current flow problem. For the following estimations the circumferential air velocity is assumed to reach $90\,\%$ of the pitch line velocity, as described by Fondelli et al. [3].

Empirical correlations have been derived for the distance y_d a liquid jet travels into the direction of the jet axis before disintegrating into droplets under the influence of a cross-flow. Wu et al. [22] propose

$$\frac{y_d}{D_{\mathrm{jet}}} = 3.07 q^{0.53} , \qquad (4)$$

where q is the momentum flux ratio

$$q = \frac{\rho_{\mathrm{jet}} V_{\mathrm{jet}}^2}{\rho_{\mathrm{air}} V_{\mathrm{air}}^2} . \qquad (5)$$

The correlation (4) was applied for the operating points in Tab. IV. It was found that the calculated values for y_d clearly exceed the maximum distance between the gear flanks and the nozzle ($\approx 12.5\,D_{\mathrm{jet}}$). Thus, no significant breakup due to the air cross-flow is to be expected.

B. Comparison of SPH to VOF

For both, the SPH and VOF setup a discretization study was conducted with 23, 46, 92, and 184 particles/cells across the jet diameter. For direct comparability an equidistant mesh was used for the VOF simulations.

The study revealed a reasonable resolution with 92 particles over the diameter for the SPH simulation, yielding $2.8 \cdot 10^6$ particles in total. Due to interpolation problems at the sliding interface the VOF simulation could not be run successfully at this resolution. Hence, the case with 46 cells per jet diameter was used in the subsequent comparison.
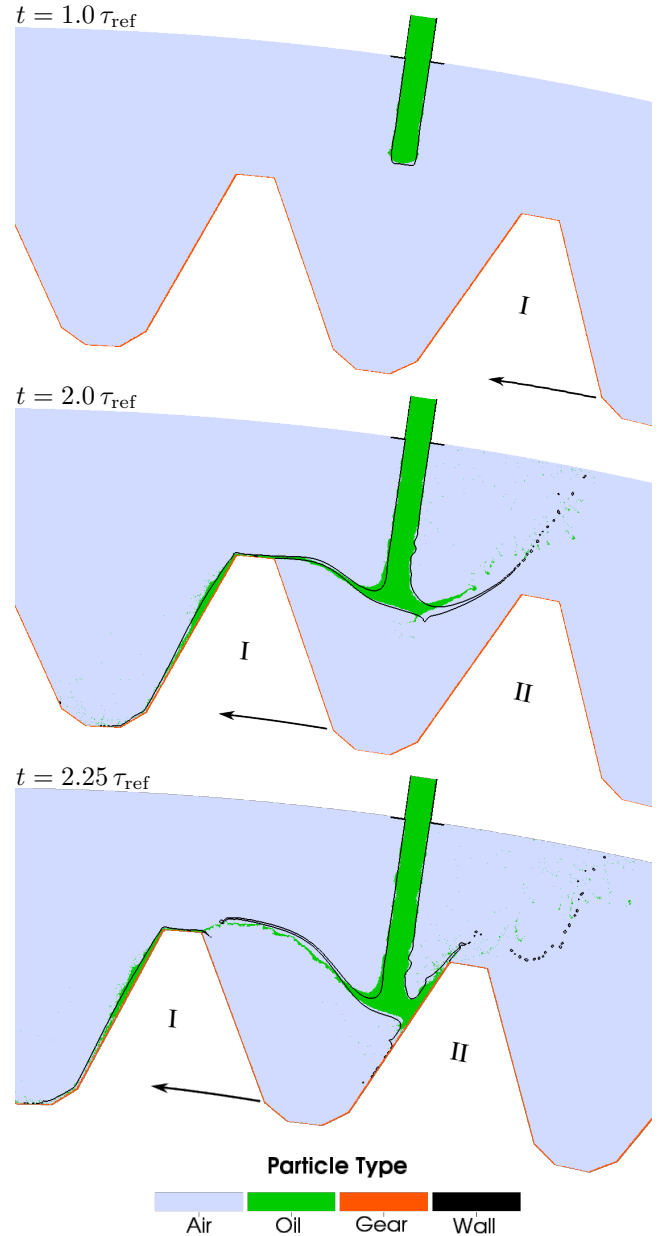

Fig. 5. Time evolution of the predicted phase distribution for the baseline case II-b at $t = 1.0/2.0/2.25\,\tau_{\mathrm{ref}}$ using SPH. The VOF results are overlaid as iso-contours (black line) of the oil volume fraction with $\alpha = 0.5$.

1) Phenomenological Comparison of the Two-Phase Flow: Comparing the time evolution of the predicted two-phase flow as displayed in Fig. 5 allows for a qualitative comparison between the SPH and VOF method. The snapshots show results for the baseline case II-b at three time steps $t = 1.0/2.0/2.25\,\tau_{\mathrm{ref}}$, where τ_{ref} is the reference time, defined by one full passing of a gear tooth through the jet axis. The VOF result is shown as iso-contour (black line) for the volume fraction of $\alpha = 0.5$.

The shape of the oil-jet compares well with the conclusions drawn from the non-dimensional considerations in Sec. IV-A, as no significant breakup is observed for the jet-air interaction. During temporal evolution the jet hits the gear tooth I and is

deformed until a curved oil sheet has formed at the tip of the jet ($t = 2.0\,\tau_{\text{ref}}$). On the right side of the jet axis the sheet starts to disintegrate into small droplets. This phenomenon is predicted slightly differently by the SPH and VOF method. On the left side of the jet axis, it is found that the oil forms a thin ligament connecting the jet tip with the oil remaining on the tooth top land. In the third snapshot ($t = 2.25\,\tau_{\text{ref}}$) the impingement on tooth II is captured. One can see that the oil-jet has penetrated into the space between teeth I and II only to a certain depth. The aforementioned ligament is still present, but has reached a critical thickness and starts to breakup. When the jet impinges, an oil film is created starting to flow downwards and upwards on the gear flank. The initial thickness of the oil film is represented similarly by both methods. From the oil film evolving through snapshot 2-3 on the left flank of tooth I, it is found that the momentum of the oil is large enough to overcome the centrifugal forces and thus oil flows radially inwards towards the gear bottom land. The predicted film thickness is similar for the SPH and VOF method. However, for both methods a finer resolution might be required to thoroughly resolve the film. Similar flow patterns are observed for the other operating points.

Although there are slight differences observable in the predicted flow field, one can conclude that the SPH and the VOF method predict the same main flow patterns of the investigated oil-gear interaction.

2) Performance Analysis: For industrial application of CFD methods, the computational time required to achieve adequate solutions is of major importance. Thus, the conducted SPH and VOF simulations are compared regarding computational effort. In the following, the comparison is shown for simulations with same spatial resolution, i.e. for runs with $\Delta x = D_{\text{jet}}/46$ and $7 \cdot 10^5$ particles/cells in total.

The required wall clock time for a defined physical simulation time of $t_{\text{sim}} = 4\tau_{\text{ref}}$ was measured for a varying number of cores, i.e. 4, 8, 16, 32, 64, and 128. For each run the average physical time calculated within one wall clock hour is shown in Fig. 6. For large numbers of cores significantly more physical time can be simulated within one wall clock hour using the SPH approach compared to the VOF method. It is apparent, that also for fewer cores SPH can compete and even outperforms VOF, e.g. by a factor of 2 for 8 cores. Compared to Braun et al. [9] the scalability of the same SPH code is slightly reduced, which is an effect of load imbalance due to the gear rotation. However, the widely acknowledged outstanding scalability of SPH also proves true for the present simulation of the oil-gear interaction, while the VOF method clearly shows performance losses for an increased number of cores.

Note that with the VOF method non-equidistant meshes and AMR [3] can be used to considerably reduce the initial cell number, leading to reduced computational costs. It was found that for the two-dimensional setups this is not significant since the scalability of VOF with AMR appeared to be poor (see
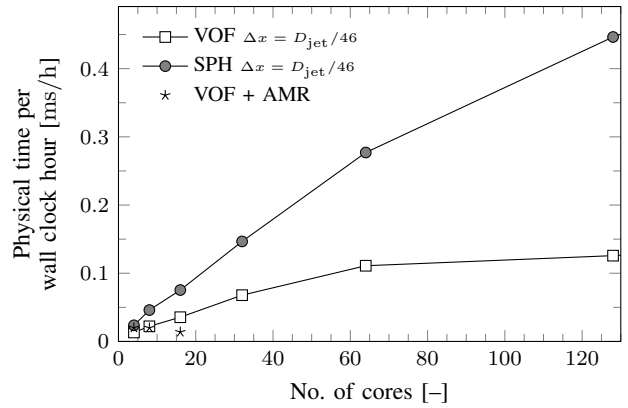

Fig. 6. Physical time per wall clock hour for SPH and VOF simulations of baseline case II-b with $7 \cdot 10^5$ particles/cells.
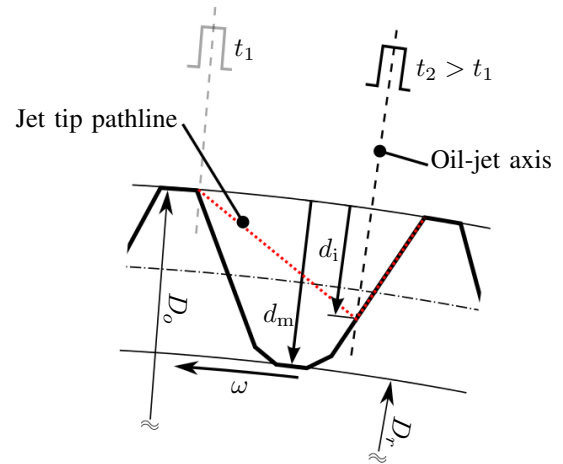

Fig. 7. Definition of the impingement depth d_{i}.

Fig. 6), however, for three-dimensional setups the effect could be more pivotal.

C. Prediction of the Impingement Depth

The impingement depth d_{i} is an important design parameter for oil-jet lubrication and cooling of gears. It is defined as depicted in Fig. 7. As illustrated, in a reference frame fixed to the gear the jet tip follows the indicated pathline (red) after passing the top land of a rotating gear tooth. The radial distance between the impact point on the next tooth flank and the outer diameter of the gear is the impinging depth d_{i}, which is here normalized by the maximum depth d_{m}.

The resulting impingement depths for the varying oil-jet velocities and rotational speeds from Tab. III are shown in Fig. 8. The values predicted by the SPH simulations are compared to analytical values, which were obtained from a simple kinematic model of the involved gear and jet motions, similar to the one by Akin and Townsend [23] for a spur gear with involute teeth. Furthermore, for cases I-b, II-b, and III-b ($V_{\text{jet}} = V_0$) the results of the VOF simulations are included.

The predicted impingement depth using SPH for $V_{\text{jet}} = V_0$ are in excellent agreement with the VOF results. As expected, a larger d_{i} for slower rotational speeds is predicted, because
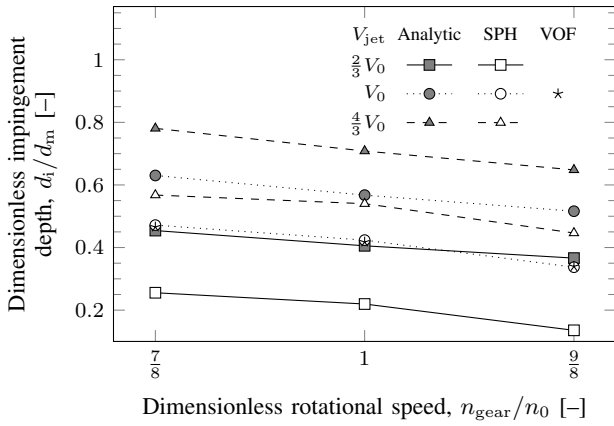
Fig. 8. Dimensionless impingement depth for all cases from Tab. III as obtained with SPH and analytically. VOF results are shown for $V_{jet} = V_0$.

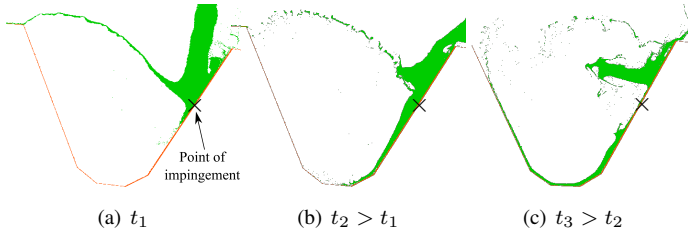(a) t_1 (b) $t_2 > t_1$ (c) $t_3 > t_2$

Fig. 9. Oil film on the left flank of gear teeth II (see Fig. 5) for three consecutive time steps of the baseline case II-b.

the jet has more time to travel radially inwards. Respectively, for larger rotational speeds d_i decreases. Comparing SPH and VOF to the analytical results an offset for all data points is observed. The impingement depths appear overestimated by the kinematic model, in which an infinitesimally thin jet is assumed and the oil-gear interaction and windage effects are neglected [23], which can shift the calculated impingement depths towards higher values. However, the relative trends compare well.

The predicted values for jet velocities of $V_{jet} = V_0$ and $V_{jet} = \frac{4}{3}V_0$ lie in a range between 0.4 and 0.6, which is considered as reasonable for sufficient cooling, whereas the slowest jet velocity results in depths below 0.3, indicating an improper oil supply to the gear.

D. Wetting Behavior

For optimal cooling and lubrication it is of major interest to cover most of the gear surface with oil. Earlier investigations [24] already mention, that the impingement depth is not the actual maximum depth the oil penetrates towards the bottom land. In fact, the impinging oil-jet will spread into two branches. One flowing radially outwards, but one pointing inwards and thus effectuate a wetting of the gear flank below the impingement point.

The described branching of the oil can also be observed for the results obtained in the present study. As can be seen from Fig. 9 showing a time series of three successive snapshots of the reference case II-b, the oil clearly covers parts of the gear
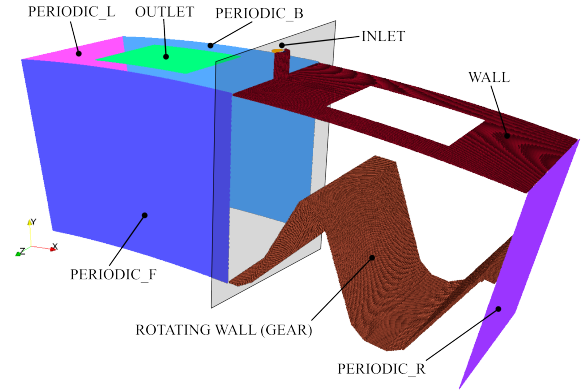

Fig. 10. 3D SPH setup. Left: Markers for inlet, outlet, and periodic BCs. Right: Static and rotating wall (gear) particles. Interior particles are not visible.

flank below the point of impingement ($\times$). Beyond that, the oil momentum is large enough to overcome the centrifugal forces and reach the bottom land of the gear (Fig. 9(b)) and start climbing up the right gear flank of the neighboring tooth (Fig. 9(c)), which also compares very well with findings by DeWinter and Blok [24] for fling-off cooling.

E. 3D Simulation

Although the 2D setup was found to be capable of revealing important flow characteristics, the investigated flow is of three-dimensional nature. Thus, it is desirable to simulate real 3D setups for comparison and determination of three-dimensional effects. The initial setup is illustrated in Fig. 10. The figure shows a split view: Markers for inlet, outlet, and periodic BCs are shown on the left side. On the right side, the fixed and rotating (gear) wall particles are visible. The interior of the domain is filled with air particles at rest. Compared to the 2D setup (cf. Fig. 3) an additional set of periodic boundary markers was used for the front (PERIODIC_F) and back (PERIODIC_B) of the domain. Furthermore, the outlet size was reduced as portions of the top surface are now modeled as slip wall. In total the setup consists of 42 million particles with $\Delta x = D_{jet}/23$.

Fig. 11 displays a snapshot of the 3D simulation at $t = 1.5\,\tau_{ref}$ for the reference case II-b. Compared to the 2D simulations (cf. inset) similar flow patterns are observed.

The successful 3D simulation demonstrates that the available set of BCs facilitates the incorporation of the gear motion even for highly complex three-dimensional cases with adjacent periodic boundaries. For future work this enables further investigations of the oil-gear interaction with the presented setup.

V. CONCLUSION

The modeling of oil-jet lubrication for spur gears using the SPH and VOF method was presented. It was shown that with the available set of BCs the presented setup can be efficiently modeled including the gear motion using SPH.

With a 2D setup the resulting flow patterns of the oil-gear interaction were predicted in good agreement with the established VOF method. At the same time, the advantages
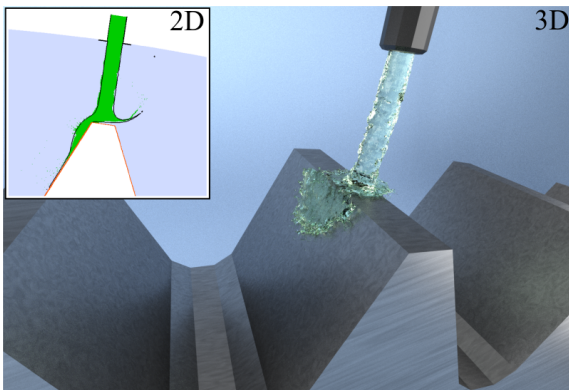
Fig. 11. Snapshot of the 3D simulation for the reference case II-b. The phase interface was extracted using the α-shapes algorithm [25] and the scene was rendered using the Cycles render engine of the graphics software Blender.

regarding the incorporation of the gear motion compared to mesh-based methods became visible.

For varied rotational speeds and jet velocities the results were compared quantitatively. It was found that the impingement depth is predicted reasonably, providing consistent values compared to the VOF method. Qualitative accordance was observed for the predicted wetting behavior. Its analysis revealed that the oil can overcome centrifugal forces and can reach the bottom land of the gear.

In general, it was shown that SPH has become a very promising tool applicable for industrially relevant systems, especially when conventional mesh-based CFD methods require non-standard features like for deforming domains or multi-phase flows. In addition, SPH was found to perform superiorly regarding computational effort especially at high and moderate number of cores, enabling highly parallelized computations.

This work presents a first step towards the simulation of more complex gearbox systems including the modeling of interlocking gears. For such a scenario the sliding interface approach of the VOF method can no longer be applied and the advantages of SPH will become even more prominent.

REFERENCES

[1] L. S. Akin, J. J. Mross, and D. P. Townsend, "Study of lubricant jet flow phenomena in spur gears," *Journal of Tribology*, vol. 97, no. 2, pp. 283–288, Apr. 1975.

[2] R. F. Handschuh, "Effect of lubricant jet location on spiral bevel gear operating temperatures," NASA, Tech. Rep. NASA/TM—105656, 1992.

[3] T. Fondelli, A. Andreini, R. Da Soghe, B. Facchini, and L. Cipolla, "Numerical simulation of oil jet lubrication for high speed gears," *International Journal of Aerospace Engineering*, vol. 2015, no. Article ID 752457, p. 13, 2015.

[4] M. Yazdani and M. C. Soteriou, "A novel approach for modeling the multiscale thermo-fluids of geared systems," *International Journal of Heat and Mass Transfer*, vol. 72, p. 517–530, 2014.

[5] M. Z. Mettichi, Y. Gargouri, P. H. L. Groenenboom, and F. el Khaldi, "Simulating oil flow for gearbox lubrication using SPH," in *Proceedings of the 10th International SPHERIC Workshop*, 2015, pp. 237–243.

[6] C. Höfler, S. Braun, R. Koch, and H.-J. Bauer, "Modeling spray formation in gas turbines – a new meshless approach," *Journal of Engineering for Gas Turbines and Power*, vol. 135, no. 1, pp. 011 503–011 503, Nov. 2012.

[7] L. Wieth, C. Lieber, W. Kurz, S. Braun, R. Koch, and H.-J. Bauer, "Numerical modeling of an aero-engine bearing chamber using the meshless smoothed particle hydrodynamics method," in *ASME Turbo Expo 2015: Turbine Technical Conference and Exposition*, no. GT2015-42316, 2015, p. V02BT39A014.

[8] L. Wieth, K. Kelemen, S. Braun, R. Koch, H.-J. Bauer, and H. P. Schuchmann, "Smoothed particle hydrodynamics (SPH) simulation of a high-pressure homogenization process," *Microfluidics and Nanofluidics*, vol. 20, no. 2, pp. 1–18, 2016.

[9] S. Braun, M. Krug, L. Wieth, C. Höfler, R. Koch, and H.-J. Bauer, "Simulation of primary atomization: Assessment of the smoothed particle hydrodynamics (SPH) method," in *13th Triennial International Conference on Liquid Atomization and Spray Systems*, 2015.

[10] G. Chaussonnet, S. Braun, L. Wieth, R. Koch, H.-J. Bauer, A. Sänger, T. Jakobs, and N. Djordjevic, "SPH simulation of a twin-fluid atomizer operating with a high viscosity liquid," in *13th Triennial International Conference on Liquid Atomization and Spray Systems*, 2015.

[11] X. Hu and N. Adams, "An incompressible multi-phase SPH method," *Journal of Computational Physics*, vol. 227, no. 1, pp. 264 – 278, 2007.

[12] A. Colagrossi and M. Landrini, "Numerical simulation of interfacial flows by smoothed particle hydrodynamics," *Journal of Computational Physics*, vol. 191, no. 2, pp. 448–475, 2003.

[13] K. Szewc, J. Pozorski, and J.-P. Minier, "Analysis of the incompressibility constraint in the smoothed particle hydrodynamics method," *International Journal for Numerical Methods in Engineering*, vol. 92, no. 4, pp. 343–369, 2012.

[14] S. Adami, X. Hu, and N. Adams, "A new surface-tension formulation for multi-phase SPH using a reproducing divergence approximation," *Journal of Computational Physics*, vol. 229, no. 13, pp. 5011–5021, 2010.

[15] S. Braun, L. Wieth, R. Koch, and H.-J. Bauer, "A framework for permeable boundary conditions in SPH: inlet, outlet, periodicity," in *Proceedings of the 10th International SPHERIC Workshop*, 2015, pp. 237–243.

[16] J. M. D. Alonso, "DualSPHysics: Towards high performance computing using SPH technique," Ph.D. dissertation, Uniersidad de Vigo, Departamento de Física Aplicada, 2014.

[17] *ANSYS® Fluent, Release 16.1, Fluent User's Guide*, ANSYS, Inc.

[18] M. J. Hill, R. F. Kunz, R. W. Noack, L. N. Long, P. J. Morris, and R. F. Handschuh, "Application and validation of unstructured overset CFD technology for rotorcraft gearbox windage aerodynamics simulation," in *64th Annual Forum of the American Helicopter Society*, 2008.

[19] M. Yazdani, M. C. Soteriou, F. Sun, and Z. Chaudhry, "Prediction of the thermo-fluids of gearbox systems," *International Journal of Heat and Mass Transfer*, vol. 81, pp. 337–346, 2015.

[20] A. H. Lefebvre, *Atomization and Sprays*, ser. Combustion (Hemisphere Publishing Corporation). Taylor & Francis, 1988.

[21] W. Ohnesorge, "Die Bildung von Tropfen an Düsen und die Auflösung flüssiger Strahlen," *Zeitschrift für angewandte Mathematik und Mechanik*, vol. 16 (6), pp. 355 – 358, 1936.

[22] P.-K. Wu, K. A. Kirkendall, R. P. Fuller, and A. S. Nejad, "Breakup processes of liquid jets in subsonic crossflows," *Journal of Propulsion and Power*, vol. 13, no. 1, pp. 64–73, Jan. 1997.

[23] L. S. Akin and D. P. Townsend, "Lubricant jet flow phenomena in spur and helical gears with modified addendums–for radially directed individual jets," NASA Center for AeroSpace Information (CASI), Tech. Rep., 1989, nASA-TM-101460.

[24] A. DeWinter and H. Blok, "Fling-off cooling of gear teeth," *Journal of Engineering for Industry*, vol. 96, no. 1, pp. 60–70, Feb. 1974.

[25] H. Edelsbrunner, D. Kirkpatrick, and R. Seidel, "On the shape of a set of points in the plane," *IEEE Transactions on Information Theory*, vol. 29, no. 4, pp. 551–559, Jul 1983.